Chemical Physics 142 (1990) 311–320
North-Holland

TWO-PHOTON DISSOCIATION OF SULFUR DIOXIDE AT 248 AND 308 nm

C.S. EFFENHAUSER, P. FELDER and J.Robert HUBER
Physikalisch-Chemisches Institut der Universität Zürich, Winterthurerstrasse 190, CH-8057 Zurich, Switzerland

Received 16 october 1989

The photodissociation of SO_2 after two-photon excitation at 248 and 308 nm has been studied by means of photofragment translational spectroscopy (PTS). With 308 nm excitation, the time-of-flight distributions of the SO photofragments exhibit high-kinetic-energy thresholds which are assigned to the formation of $SO(X\,^3\Sigma^-)+O(^3P)$, $SO(X\,^3\Sigma^-)+O(^1D)$, and $SO(a\,^1\Delta)+O(^3P)$. A weak vibrational structure indicates the production of $SO(a\,^1\Delta)$ molecules in vibrational states up to at least $v=8$. After excitation at 248 nm, nine different primary processes are clearly identified leading to SO+O as well as to $S+O_2$ fragments in various electronic states. All observed kinetic energy thresholds conform to a dissociation energy $D_0=543$ kJ/mol (45400 cm^{-1}) for the reaction $SO_2\rightarrow SO+O$ and $D_0=569$ kJ/mol (47600 cm^{-1}) for the reaction $SO_2\rightarrow S+O_2$. Evidence was found for the formation of higher SO electronic states in the energy region 28000–31000 cm^{-1}, in particular for the previously not observed $SO(A''\,^3\Sigma^+)$ state which possesses a term energy T_0 close to 30000 cm^{-1}. Furthermore, the PTS method, in providing a direct way to determine the electronic states of each individual fragment of a fragment pair, revealed that the spin is not conserved in the $SO_2\rightarrow SO+O$ dissociation.

1. Introduction

The primary process of the photolysis of sulfur dioxide

$$SO_2 \xrightarrow{h\nu} SO+O \qquad (1)$$

following excimer laser excitation at 193 nm has been studied extensively under collisionless conditions [1–3]. The photofragments are formed in the electronic ground state and the decay mechanism has been proposed to be predissociation. Based on the sudden decrease of the fluorescence yield and the fluorescence lifetime, the dissociation energy D_0 was determined to be 543 kJ/mol (45400 cm^{-1}) [4]. Less is known about the photodissociation processes from higher excited electronic states of SO_2. The VUV spectrum recorded between 220 and 105 nm [5] revealed several diffuse absorption bands below 135 nm which were attributed to transitions to a Rydberg system [5,6]. A weaker absorption band between 135 and 160 nm has not yet been assigned. The gas phase photochemistry of SO_2 after excitation at 116.5, 123.6, and 147 nm has been investigated by Lalo and Vermeil [7], who reported evidence of the production of sulfur atoms in the electronic states ^3P and ^1D according to the primary reaction

$$SO_2 \xrightarrow{h\nu} S+O_2\,. \qquad (2)$$

A particularly convenient way to create highly excited SO_2 molecules can be achieved by a resonant two-photon absorption process as indicated in the energy level scheme of fig. 1. Using a laser pulse of a few nanoseconds duration, absorption of a first UV photon leads to the mixed $\tilde{B}$–$\tilde{A}$ state which, favored by its long lifetime (10^1–10^2 μs) [8], can absorb a second photon of the same laser pulse. This excitation mode has been used at 248 nm by Wilson et al. [9], who observed the formation of $SO(X\,^3\Sigma^-)$ and $S(^3P)$ in the electronic ground state by utilizing the same laser pulse to probe the fragments with the LIF method. Under the same excitation conditions also Fotakis et al. [10] reported the production of $SO(X\,^3\Sigma^-)$. Wildt et al. [11] used 248 nm excitation for the production of the $SO(b\,^1\Sigma^+)$ species and proposed a mechanism that involves either a resonant two-photon absorption or a one-photon absorption by the parent followed by a chemical reaction with a ground state SO_2 molecule. With two photons

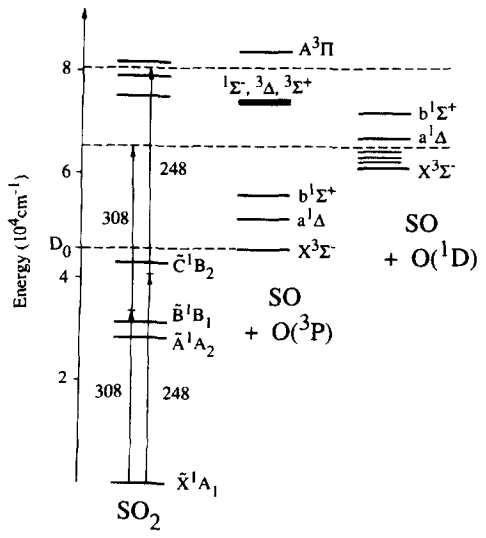

Fig. 1. Energy level scheme illustrating the energetics of the formation of SO+O fragments in various electronic states after two-photon dissociation of SO_2 at 248 and 308 nm. The three highest indicated electronic states of SO_2 around 80000 cm^{-1} have been assigned as Rydberg states. Some vibrational levels are shown for the production of $SO(X\,^3\Sigma^-)+O(^1D)$ atoms.

in the 285–311 nm region, Venkitachalam and Bersohn [12] identified by LIF detection the dissociation products $SO(X\,^3\Sigma^-)$ and $S(^3P, ^1D)$.

In the present work we report results of a comprehensive two-photon dissociation study on SO_2 using excimer laser excitation at 248 and 308 nm. The experiments were carried out under collisionless conditions, using a high resolution time-of-flight apparatus equipped with a rotatable pulsed molecular beam source. The photofragments SO, O, S, and O_2 were found to be produced in various electronic states according to the schemes:

$$\begin{aligned} SO_2 &\xrightarrow{308} SO_2(\tilde{B}, \tilde{A}) \\ &\xrightarrow{308} SO_2^* \rightarrow SO(X\,^3\Sigma^-)O(^3P) \\ &\qquad \rightarrow SO(a\,^1\Delta)+O(^3P) \\ &\qquad \rightarrow SO(X\,^3\Sigma^-)+O(^1D)\,, \end{aligned}$$

$$\begin{aligned} SO_2 &\xrightarrow{248} SO_2(\tilde{B}) \\ &\xrightarrow{248} SO_2(\tilde{G}) \rightarrow \left.\begin{matrix} SO(X\,^3\Sigma^-) \\ SO(a\,^1\Delta) \\ SO(b\,^1\Sigma^+) \end{matrix}\right\} + \begin{cases} O(^3P) \\ O(^1D)\,, \end{cases} \\ SO_2(\tilde{G}) &\rightarrow O_2(X\,^3\Sigma_g^-)+S(^3P) \\ &\rightarrow O_2(X\,^3\Sigma_g^-)+S(^1D) \\ &\rightarrow O_2(a\,^1\Delta_g)+S(^1D)\,. \end{aligned} \qquad (3)$$

These primary processes were identified by the high-kinetic-energy thresholds observed in the photofragment time-of-flight (TOF) distributions. Further energy thresholds can be assigned to the formation of higher electronic states of SO, notably the previously not observed $A''\,^3\Sigma^+$ state.

2. Experimental

The experiments were performed with an apparatus consisting of a pulsed molecular beam source, a high vacuum scattering chamber, and a quadrupole mass spectrometer. The pulsed molecular beam was generated with a home-built piezoelectric valve with a 0.3 mm diameter orifice. The beam source is located within a differentially pumped vacuum chamber which can be rotated about the propagation direction of the photodissociation laser. After a flight path of 34.5 cm the photofragments were ionized, mass selected and detected by means of a quadrupole mass spectrometer (Balzers QMA 160). The electron bombardment ionizer of the latter was housed in a triply differentially pumped UHV chamber with a vacuum of 2×10^{-10} mbar. A multichannel scaler (800 channels, 1 μs dwell time) was used to measure the arrival time distribution of the detected ions. The time-of-flight distribution of the neutral photofragments was obtained by subtraction of a small time offset resulting from the transit time of the ions through the mass filter.

The rare gas halide excimer laser (Lambda Physik EMG 101 MSC) provided a pulse energy of 300 mJ at 248 nm (KrF* emission) and 70 mJ at 308 nm (XeCl* emission). The unpolarized laser light was focused to a spot size of about 3 mm×3 mm giving

rise to a peak intensity of 200 MW/cm^2 and 45 MW/cm^2, respectively. Most of the experiments were performed using a mixture of 5% SO_2 seeded in helium at a stagnation pressure of 400 mbar. In some experiments at 248 nm, a 25% mixture in helium at a stagnation pressure of 100 mbar or a 5% mixture in neon at 400 mbar was used. The velocity distribution of the molecular beam was determined by the method of laser induced hole burning yielding a most probable beam velocity of 1310 and 755 m/s with associated full-width-at-half-maximum (fwhm) values of 11 and 35% for the 5 and 25% mixture in helium, respectively. In the case of the neon mixture a value of 765 m/s and a fwhm of 9% was obtained.The translational energy resolution of a TOF experiment depends on experimental parameters like the detection angle, the velocity distribution of the molecular beam, and on the translational energy itself. Typical values are ± 500 to 1000 cm^{-1} in the high-kinetic-energy part of the spectra and ± 300 cm^{-1} in the low-kinetic-energy region.

The pulsed molecular beam and the laser were operated with a repetition rate of 40 Hz. Photofragment TOF distributions were recorded at several molecular beam angles Θ, with the mass filter set at $m/e=32$ and 48. The TOF signal at $m/e=48$ originates from the SO photofragments produced in reaction (1). The S and O_2 fragments from reaction (2) are detected at $m/e=32$ but the resulting spectra are complicated by the overlap with a signal from SO which contributes by way of its ionization product S^+. Typical photofragment count rates were one count per laser shot at the smaller detection angles $\Theta=15$ and 21° and 0.3–0.5 counts per shot at the larger detection angles $\Theta=36$ and 45°. In order to obtain a satisfactory signal to noise ratio 150000–840000 laser shots were accumulated for each TOF distribution.

3. Results

3.1. Photodissociation at 308 nm

The TOF distributions of the SO photofragments recorded at this excitation wavelength are shown in fig. 2. Several kinetic energy thresholds are distinctly resolved in the TOF distributions and are assigned to a two-photon dissociation of SO_2 leading to oxygen atoms and sulfur monoxide in various electronic and vibrational states. The assignment is based on the fact

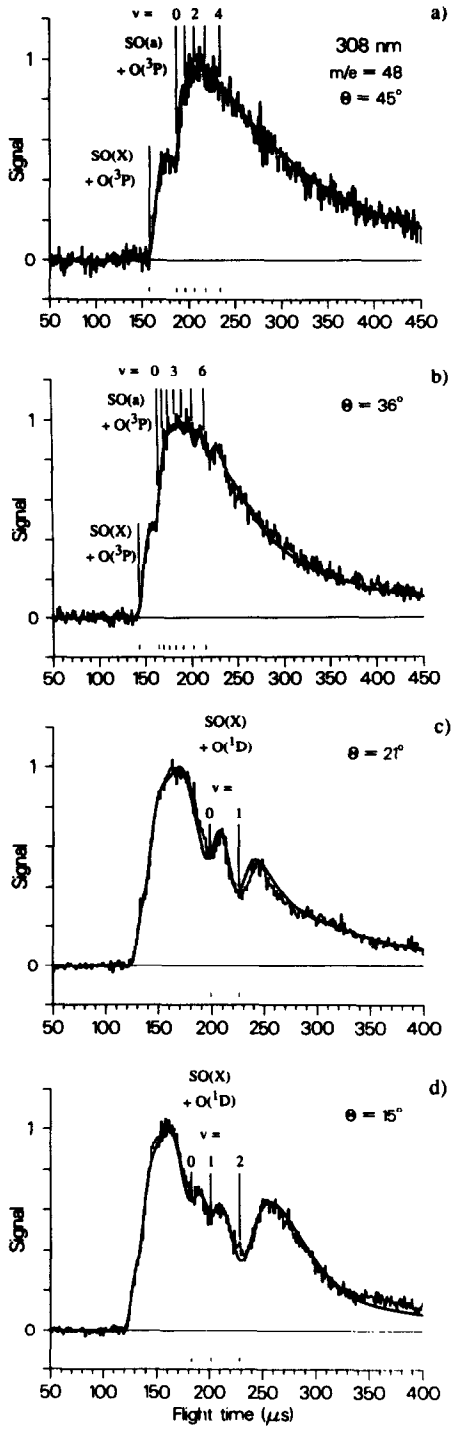

Fig. 2. Two-photon dissociation of SO_2 at 308 nm: TOF distributions of the SO photofragments ($m/e=48$) recorded at detection angles $\Theta=15$, 21, 36, and 45°. The solid lines are calculated with the $P(E_T)$ function shown in fig. 3.

that all observed high-kinetic-energy thresholds are in excellent agreement with those calculated from the known values of the electronic and vibrational excitation energies of the fragments by applying the conservation of energy

$$E_T = 2h\nu - D_0 - E_{el} - E_{vib} - E_{rot} . \quad (4a)$$

Here, E_T denotes the total translational energy of the fragment pair, E_{el} the total electronic excitation energy of both fragments, and E_{vib} and E_{rot} the vibrational and rotational energy of the diatomic fragment respectively. For the diatomic fragments in the vibrational and rotational ground state (or low J states according to the resolution of our apparatus) the kinetic energy becomes

$$E_T = 2h\nu - D_0 - E_{el} \quad (4b)$$

and is identical to the high-kinetic-energy threshold for the formation of the fragment pair in the electronic state specified by E_{el}. In a similar way, the high-kinetic-energy thresholds for the production of rotationally cold diatomic fragments in specified vibrational states are given by

$$E_T = 2h\nu - D_0 - E_{el} - E_{vib} . \quad (4c)$$

The total translational energy of the fragment pair is calculated from the kinetic energy of the detected fragment using linear momentum conservation. The high-kinetic-energy thresholds indicated in figs. 2a–2d are calculated from a single Newton diagram using the most probable molecular beam velocities that are given in section 2. Under our experimental conditions (pulsed supersonic molecular beams of SO_2 seeded in rare gases), the internal energy of the SO_2 parent molecules can be neglected in eq. (4).

The TOF distributions recorded at $\Theta = 45°$ (fig. 2a) and $\Theta = 36°$ (fig. 2b) show two thresholds at flight times corresponding to total translational energies E_T of 19500 and 13600 cm^{-1}. The first threshold indicates the formation of both fragments in their electronic ground states, i.e. $SO(X\,^3\Sigma^-)$ and $O(^3P)$, whereas the second one can be attributed to electronically excited $SO(a\,^1\Delta)$ produced in coincidence with $O(^3P)$ atoms. An additional dissociation channel is observed at $\Theta = 21°$ (fig. 2c) and $\Theta = 15°$ (fig. 2d). These TOF spectra exhibit several components which result from the production of excited $O(^1D)$ atoms and $SO(X\,^3\Sigma^-)$ in the vibrational states $v = 0$, 1, and 2. The formation of $v = 3$ is energetically also possible, but these slow photofragments are hardly detectable with our apparatus due to the relatively large molecular beam background at the small detection angle required.

The solid lines in fig. 2 are TOF distributions calculated with the translational energy distribution $P(E_T)$ shown in fig. 3. This calculation takes into account the transformation from the laboratory to the center-of-mass reference frame and all known experimental effects influencing the resolution of the measured TOF distributions, namely the angular divergence of the molecular and photofragment beams (2.2° and 0.8°, respectively), the effective ionizer length (5 mm), the size of the laser focus (3 mm × 3 mm), and the velocity distribution of the molecular beam. The $P(E_T)$ function was chosen as a superposition of the form [13]

$$P(E_T) = \sum_i C_i (B_i - E_T)^{\beta_i} (E_T - A_i)^{\alpha_i} . \quad (5)$$

This type of function has well defined lower and upper energy thresholds A_i and B_i respectively, and a sufficiently flexible shape owing to adjustable exponents. The values for B_i were determined from the energy conservation via eq. (4) using the electronic excitation energies listed in table 1 and the vibrational energies E_{vib} calculated from $\omega_e = 1151$ cm^{-1} and $\omega_e x_e = 6.4$ cm^{-1} [16] in the case of $SO(X\,^3\Sigma^-)$

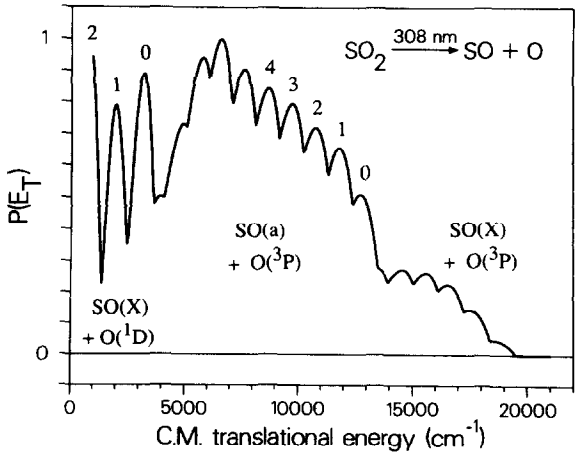

Fig. 3. Two-photon dissociation of SO_2 at 308 nm: photofragment translational energy distribution $P(E_T)$ of reaction (1) in the center-of-mass reference frame. Some vibrational states of SO are indicated.

Table 1
Threshold energies [a] for the formation SO+O and O_2+S fragments in various electronic states [b]

	$O(^3P)$	$O(^1D)$	$O(^1S)$
$SO(X\,^3\Sigma^-)$	0	15868	33793
$SO(a\,^1\Delta)$	5862	21730	39655
$SO(b\,^1\Sigma^+)$	10469	26337	44262
$SO(A\,^3\Pi)$	38293	54161	72086
	$S(^3P)$	$S(^1D)$	$S(^1S)$
$O_2(X\,^3\Sigma_g^-)$	0	9239	22180
$O_2(a\,^1\Delta_g)$	7882	17121	30062
$O_2(b\,^1\Sigma_g^+)$	13121	22360	35301

[a] The energies are given relative to the ground state fragments.
[b] The data were taken from the refs. [14,15], the energy unit is cm^{-1}.

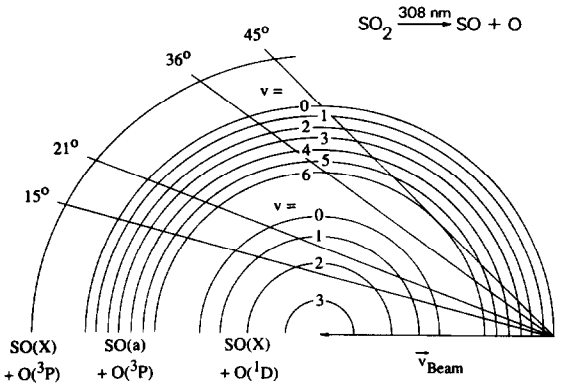

Fig. 4. Newton diagram illustrating the kinematics for the detection of the SO photofragments in various vibrational states formed by two-photon dissociation at 308 nm. The circles represent the maximum recoil velocities for the indicated primary processes.

and from $\omega_e = 1115\ cm^{-1}$ and $\omega_e x_e = 6.8\ cm^{-1}$ [17] in the case of $SO(a\,^1\Delta)$.

The vibrational structure resulting from the production of $O(^1D)+SO(X\,^3\Sigma^-)$ is well resolved and allows us to determine the rotational energy distribution in $v=0$ and 1. For $v=2$ only the rotationally colder part is detectable at $\Theta = 15°$ as illustrated by the Newton diagram in fig. 4. The rotational energy distribution is narrow and nearly the same for $v=0$ and 1 with a fwhm of $\approx 500\ cm^{-1}$ and a maximum which, according to the rotational constant of SO [18], corresponds to $J \approx 26$ for both vibrational states.

The TOF distributions recorded at $\Theta = 45$ and 36° (figs. 2a and 2b) show evidence of a weak vibrational progression of the $SO(a\,^1\Delta)$ fragments up to at least $v=8$. The branching ratio of the three dissociation channels observed can be estimated from the $P(E_T)$ distribution displayed in fig. 3 as

$$SO(X\,^3\Sigma^-)+O(^3P) : SO(a\,^1\Delta)+O(^3P) : SO(X\,^3\Sigma^-)+O(^1D) \approx 1:2:1\,.$$

No energy threshold is discernible for the formation of $SO(b\,^1\Sigma^+)+O(^3P)$, although it is energetically possible. However, a minor contribution from this channel cannot be excluded.

Additional TOF distributions were measured at $m/e = 32$. As already mentioned, at this m/e ratio S and O_2 fragments formed in reaction (2) should be detectable as well as SO fragments originating from reaction (1). These TOF distributions (not shown here) have contributions from fast photofragments which can only be formed in reaction (2). (Although reaction (2) is slightly more endothermic than reaction (1), the fragments formed in reaction (2) can reach a higher recoil velocity than the heavier SO fragment.) However, no obvious kinetic energy thresholds are detected in the high kinetic energy parts of these spectra.

3.2. Photodissociation at 248 nm

The experiments at 248 nm were carried out with the mass filter settings $m/e = 32$ and 48 using various detection angles Θ. Selected TOF distributions are displayed in figs. 5–7. The spectra are highly structured and allow the identification of several dissociation channels. The energetics of all the observed high kinetic energy thresholds conforms with a resonant two-photon dissociation process. Unfortunately, extraction of a branching ratio for reaction (1) is not possible due to the strong overlaps from contributions of the different reaction channels.

The spectrum of fig. 5a, recorded at $m/e = 48$ with $\Theta = 36°$, shows a steep threshold at 115 μs ($E_T = 35000\ cm^{-1}$) due to the formation of $SO(X\,^3\Sigma^-)$ and $O(^3P)$. At increasingly longer flight times further kinetic energy thresholds indicate the formation of $SO(a\,^1\Delta)+O(^3P)$, $SO(b\,^1\Sigma^+)+O(^3P)$, $SO(X\,^3\Sigma^-)+O(^1D)$, $SO(a\,^1\Delta)+O(^1D)$ and

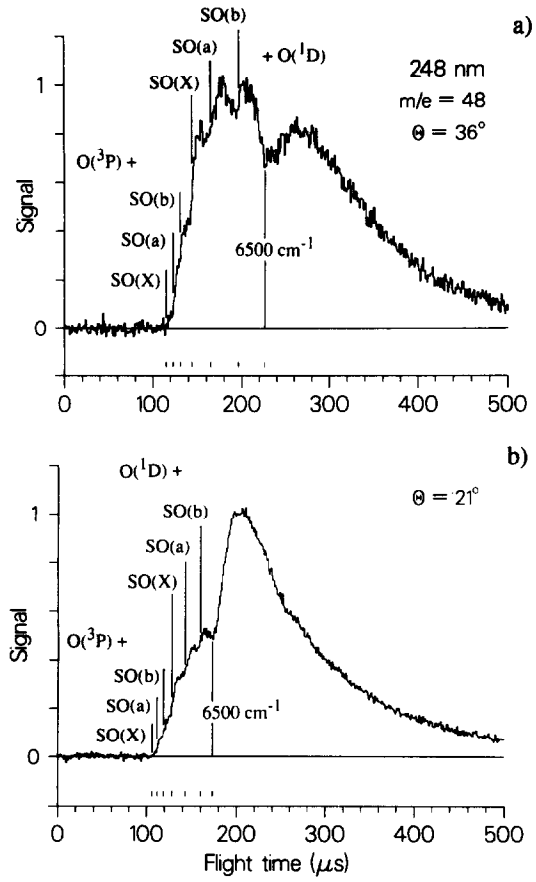

Fig. 5. Two-photon dissociation of SO_2 at 248 nm: TOF distributions recorded at $m/e=48$, $\Theta=21$ and 36°. The calculated high kinetic energy thresholds for the formation of oxygen atoms and sulfur monoxide molecules in various electronic states are indicated.

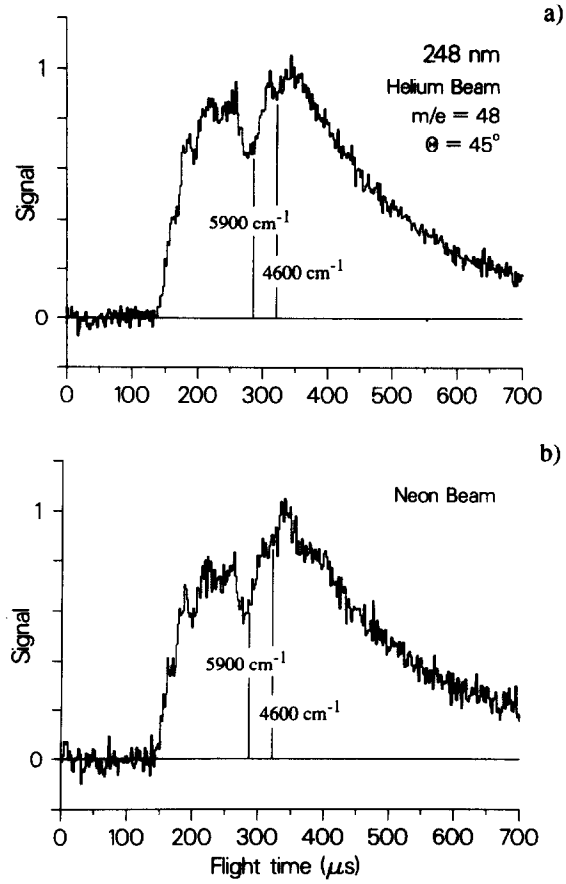

Fig. 6. Two-photon dissociation of SO_2 at 248 nm. TOF distribution recorded at $m/e=48$, $\Theta=45°$, using (a) a 25% mixture of SO_2 in helium and (b) a 5% mixture of SO_2 seeded in neon as carrier gas. Several high kinetic energy thresholds and the corresponding translational energies E_T are indicated.

$SO(b\,^1\Sigma^+)+O(^1D)$. An additional, prominent threshold is observed at ≈ 250 μs with an associated translational energy E_T of ≈ 6500 cm^{-1}. The same features are observed at correspondingly shorter flight times in the TOF distribution measured at $\Theta=21°$ as indicated in fig. 5b. Two further steps corresponding to $E_T \approx 4600$ and 5900 cm^{-1} are discernible at $\Theta=45°$ (figs. 6a and 6b). As will be discussed in section 4, these thresholds are attributed to the formation of SO fragments in higher electronic states in coincidence with ground state oxygen atoms. The generation of oxygen atoms in the higher excited ^1S state in combination with ground state SO molecules is also energetically allowed, but these fragments would possess merely about 1200 cm^{-1} of available energy and are, therefore, hardly detectable in our experiment.

In order to detect photofragments from reaction (2), several TOF distributions were recorded at a mass filter setting of $m/e=32$. As shown in figs. 7a and 7b for $\Theta=36$ and 21°, new components with high recoil velocity are found. These are assigned to the following dissociation products: $S(^3P)+O_2(X\,^3\Sigma_g^-)$, and $S(^1D)+O_2(a\,^1\Delta_g)$. Evidence of further dissociation channels leading to higher excited states of S and O_2 is prevented by the strong superposition of the contributions from reactions (1) and (2).

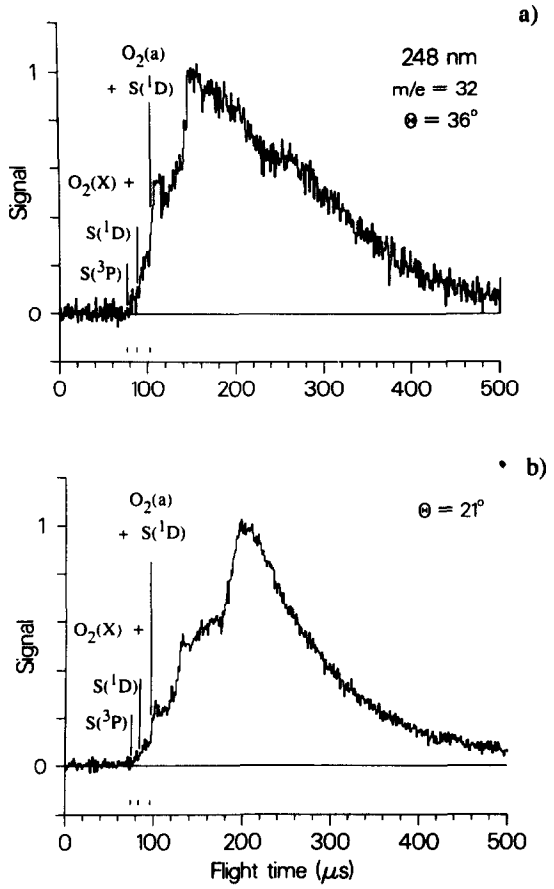

Fig. 7. Two-photon dissociation of SO_2 at 248 nm: TOF distribution recorded at $m/e=32$, $\Theta=21$ and 36°. The calculated high kinetic energy thresholds for the production of sulfur atoms and oxygen molecules in various electronic states are indicated.

4. Discussion

4.1. General remarks

The results of this investigation confirm that highly excited SO_2 molecules are readily generated via resonant two-photon excitation at 308 or 248 nm even in a beam experiment. The large fluence of a pulsed excimer laser overcomes the small absorption cross section ($\sigma_{308}\approx 3\times10^{-19}$ cm^2; $\sigma_{248}\approx 8\times10^{-20}$ cm^2) of the first excitation step. Under our experimental conditions, approximately 35% (248 nm) and 30% (308 nm) of SO_2 molecules in the interaction volume are promoted to a bound intermediate state. This state has a strongly mixed $\tilde{B}(^1B_1)$-$\tilde{A}(^1A_2)$ character arising from vibronic coupling, mainly through the $\nu_3(b_2)$ mode [8]. The spectroscopic features of the complex structure of the UV absorption spectrum in the 308–248 nm region and the dynamics, in particular the unusually long fluorescence lifetime, have been reviewed [8]. The cross section for the second excitation step at 248 nm was estimated by Wilson et al. [9] to be larger than 10^{-18} cm^2. Hence, the second absorption process is saturated under our excitation conditions and the same should be the case for the second absorption step at 308 nm according to the pronounced depletion of the molecular beam measured in our hole-burning experiments.

The dissociation energy of reaction (1) has been determined experimentally to be $D_0=543$ kJ/mol (45400 cm^{-1}) and that of reaction (2) is $D_0=569$ kJ/mol (47600 cm^{-1}) based on known thermodynamic data [14]. Our results corroborate both values as all of the observed kinetic energy thresholds can be fit accurately with these dissociation energies. Thus, following excitation into the high energy region at 64900 cm^{-1} (2×308.1 nm) or 80400 cm^{-1} (2×248.8 nm), SO_2 undergoes dissociation with a large amount of excess energy. At 308 nm photofragments are generated with an energy of 19500 cm^{-1} (reaction (1)) and 17300 cm^{-1} (reaction (2)) while at 248 nm the corresponding values are 35000 and 32800 cm^{-1}, respectively. This excess energy is equal to the available energy that is distributed among the various degrees of freedom of the photofragments. The electronically excited product states that are energetically accessible in our experiments can be drawn from table 1 (cf. fig. 1).

4.2. Photodissociation at 308 nm

Venkitachalam and Bersohn [12] have explored the photochemistry of SO_2 in the wavelength region 285–311 nm and have shown by LIF detection that $SO(X\,^3\Sigma^-)$ and sulfur atoms in the electronic states ^3P and ^1D are formed consistent with a two-photon dissociation process. Our TOF spectra revealed that upon 308 nm excitation the photofragments SO and O are produced by three different dissociation channels, namely

(1) $SO(X^3\Sigma^-)+O(^3P)$,

(2) $SO(a^1\Delta)+O(^3P)$,

(3) $SO(X^3\Sigma^-)+O(^1D)$.

The electronically excited $SO(a^1\Delta)$ fragments are also vibrationally excited (up to at least $v=8$, cf. figs. 2a and 2b) showing that two-photon dissociation at 308 nm is a suitable method for the preparation of this reactive species. The branching ratio of the three channels is estimated to be 1:2:1, i.e. about equal amounts of ground state $SO(X^3\Sigma^-)$ and electronically excited $SO(a^1\Delta)$ are produced in the primary process. The majority of the photofragments is formed as pairs of a singlet and a triplet state fragment (total spin $S=1$) thus implying heavy admixture of triplet character in the excitation or dissociation process. This is not surprising in view of the strong spin–orbit coupling in sulfur containing molecules (heavy atom effect).

A part of the TOF signal at $m/e=32$ must originate from S and O_2 photofragments formed in reaction (2). At 308 nm excitation this channel is, however, much less important than the one leading to SO+O. It is interesting to note that this finding agrees with the result of Lalo and Vermeil [7], who studied the one-photon process by exciting SO_2 at 147 nm. The low relative yield of reaction (2) might be associated with a high energy barrier involved in the formation of a cyclic transition state following one- or two-photon absorption into the 150 nm region of SO_2.

4.3. Photodissociation at 248 nm

Using two-photon excitation at this wavelength, previous studies have demonstrated that $SO(X^3\Sigma^-)$ [9,10] and $S(^3P)$ [9] are the primary dissociation products. In addition, Lalo and Vermeil [7] have found evidence for the formation of $S(^3P)$ and $S(^1D)$ after one-photon excitation of SO_2 at 123.6 nm. New information revealing the complexity of this reaction system are obtained from the TOF distributions shown in figs. 5–7. Kinetic energy thresholds clearly indicate the production of SO in the electronic states $X^3\Sigma^-$, $a^1\Delta$, and $b^1\Sigma^+$, each one formed in combination with (^3P) as well as $O(^1D)$. In addition to these six reactions, further thresholds evident in the TOF distributions of the SO fragments imply the existence of further channels. These thresholds are located in the translational energy region between 4000 and 7000 cm^{-1}, which corresponds to an internal energy range 28000–31000 cm^{-1}.

Sulfur monoxide is proposed to possess three electronic states in the region between 28000 and 31000 cm^{-1}, namely one singlet state, denoted by $c^1\Sigma^-$, and two triplet states $A'^3\Delta$ and $A''^3\Sigma^+$ (cf. fig 1 top). These states arise from the same electronic $...(\pi)^3(\pi^*)^3$ configuration. However, there exists still some ambiguity about the accurate term energies. Experimental information about the $c^1\Sigma^-$ state has been obtained from chemiluminescence spectra assigned to the $c^1\Sigma^-(v'=0)\rightarrow a^1\Delta(v'')$ transition of SO. Due to different vibrational labelling, Lee and Pimentel [19] deduced a value for the 0–0 transition of $\nu_{00}=21363$ cm^{-1}, whereas Tevault and Smardzewski [20] obtained $\nu_{00}=22540$ cm^{-1}. After the addition of the experimental term value of the $SO(a^1\Delta)$ state, $T_0=5862$ cm^{-1} [15], the above choices for ν_{00} lead to term values of the c state of 27225 and 28402 cm^{-1}, respectively. A second band system was found by Tevault and Smardzewski [20] and was assigned to the $A'^3\Delta(v'=0)\rightarrow X^3\Sigma^-(v'')$ transition with a term value $T_0=28400\pm1150$ cm^{-1} for the A′ state. Again, the error bounds arise from an uncertainty in the vibrational numbering. Furthermore, these authors could not strictly rule out the A″ state to be responsible for the observed band system. In order to clarify the contradictions in the interpretations of these experimental results, Swope et al. [21] performed CI ab initio calculations and found for the c, A′, and A″ states the following excitation energies T_e relative to the minimum of the potential energy curve of the ground state: $T_e(c^1\Sigma^-)=28100$ cm^{-1}, $T_e(A'^3\Delta)=29200$ cm^{-1}, and $T_e(A''^3\Sigma^+)=30200$ cm^{-1} (error bounds ±300 cm^{-1}). After subtraction of the energy difference T_e-T_0 (ω_e was calculated to be about 700 cm^{-1} for all these excited states [21]) the energies of the 0–0 transition are predicted to be 27900, 29000 and 30000 cm^{-1}.

At this point we note that internal energy thresholds at 28500, 29100 and 30400 cm^{-1} were detected in the $m/e=48$ TOF distributions shown in figs. 5–7. The excellent agreement between these measured values and those predicted by the calculation, permits us to assign the threshold at 30400 cm^{-1} to the

formation of $SO(A''\,^3\Sigma^+)$ in coincidence with $O(^3P)$ atoms. The other two thresholds cannot be assigned unambiguously. The calculated term energies would suggest that the threshold at 28500 cm^{-1} is due to the formation of $SO(c\,^1\Sigma^-)$ and the threshold at 29100 cm^{-1} to the formation of $SO(A'\,^3\Delta)$, both in combination with $O(^3P)$ atoms. Consequently, the vibrational labelling of the c→a transition in ref. [20] would be the correct choice, leading to $T_0 = 28400$ cm^{-1} for the $c\,^1\Sigma^-$ state. In accordance with such an assignment, the A'→X transition should be described by shifting the vibrational quantum numbers by one unit thus yielding a term value at the upper error limit which is $T_0(A'\,^3\Delta) = 29500\ cm^{-1}$.

The fact that a large part of the fragments are formed as pairs of singlet and triplet states indicates strong singlet–triplet mixing in the Rydberg $\tilde{G}$ state excited by two 248 nm photons. The contribution of reaction (2) is much larger at this excitation wavelength compared to 308 nm. From the many processes which are energetically allowed, the formation of $O_2(X\,^3\Sigma_g^-) + S(^3P)$ and of excited $O_2(a\,^1\Delta_g) + S(^1D)$ can be unambiguously derived from the TOF distributions of fig. 7. A further threshold corresponding to $E_T = 9000$ cm^{-1} is most probably due to the formation of $O_2(X\,^3\Sigma_g^-) + S(^1D)$ with a possible additional contribution of $O_2(a\,^1\Delta_g) + S(^3P)$ (cf. threshold energies given in table 1).

4.4. Final remarks

The discussion of our experimental results is based on the observation of numerous thresholds in the TOF distributions of the photofragments of SO_2. The thresholds were found to agree well with the energetics involved with the formation of SO, O, S and O_2 in their known electronic states and were taken as evidence for the production of these species. For an accurate determination of these thresholds, an appreciable fraction of the fragments has to be produced in $v = 0$ and in low rotational states. Since the TOF distribution reflects the total internal energy distribution of both fragments [22], the occurrence of distinct thresholds is favored when small fragments are produced, like a diatomic molecule and an atom in the dissociation of SO_2. The relatively large excitation energy of $O(^1D)$ implies that in the case of reaction (1) the contributions from $O(^1D)$ do not overlap with those from the lower electronically excited states of SO, simplifying the TOF spectra considerably. As discussed above, additional thresholds were detected at long flight times in the TOF distributions at $m/e = 48$ and were attributed to higher electronic states of SO.

Finally, we note that all the energy thresholds observed in our TOF spectra agree with the dissociation energies of reactions (1) and (2) (cf. section 4.1). In particular, the maximum translational energy release upon formation of ground state SO and O fragments was determined using three different excitation conditions, namely 193 nm (via the $\tilde{C}$ state) [3], at 2×308 nm, and at 2×248 nm. The observed kinetic energies of 6300, 19500 and 35000 cm^{-1}, respectively, are all consistent with $D_0 = 45400\ cm^{-1}$.

5. Conclusion

The present work provides a detailed picture of the numerous primary photochemical processes that occur after excitation of SO_2 into high electronic states at about 8 and 10 eV. Essentially all energetically allowed channels of reaction (1) are found to be operative. The pronounced "nonselectivity" (also with respect to electron spin) suggests that potential energy surface crossings and strong spin–orbit coupling are effective, notably following preparation of the Rydberg state with two 248 nm photons.

Previous studies have shown that both reactions (1) and (2) take place after two-photon excitation at 248 and 308 nm by identifying the products $X\,^3\Sigma^-$ [9,10] and $S(^3P)$ [9] and $SO(X\,^3\Sigma^-)$ and $S(^3P, ^1D)$ [12], respectively. Our TOF distributions revealed that SO photofragments are also produced in a variety of electronically excited states in combination with oxygen atoms formed in the ^3P and ^1D state as summarized in the reaction scheme (3). Most importantly, we showed in which electronic states the fragment *pairs* were produced in the primary processes. This information is a consequence of the linear momentum conservation that correlates the velocity of the detected fragment with the total internal energy of the fragment pair. Knowledge about this correlation is a prerequisite to determine whether the total spin is conserved in a photodissociation process and it can be obtained in a very direct way from a high

resolution velocity experiment carried out with e.g. the PTS method. Moreover, since the detection sensitivity of this method is essentially independent of the electronic state of the fragment being probed (in contrast to most spectroscopic techniques), the branching ratios of the various reaction channels can also be extracted from such measurements. Finally, information about the term energies of several higher electronic states of SO was obtained.

Acknowledgement

Financial support of this work by the Schweizerischer Nationalfonds zur Förderung der wissenschaftlichen Forschung and by the Alfred Werner Legat is gratefully acknowledged.

References

[1] M. Kawasaki and H. Sato, Chem. Phys. Letters 139 (1987) 585;
M. Kawasaki, K. Kasatani, H. Sato, H. Shinohira and N. Nishi, Chem. Phys. 73 (1982) 377.
[2] H. Kanamori, J.E. Butler, K. Kawaguchi, C. Yamada and E. Hirota, J. Chem. Phys. 83 (1985) 611.
[3] P. Felder, C.S. Effenhauser, B.M. Haas and J.R. Huber, Chem. Phys. Letters 148 (1988) 417.
[4] T. Ebata, O. Nakazawa and M. Ito, Chem. Phys. Letters 143 (1988) 31.
[5] D. Golomb, K. Watanabe and F.F. Marmo, J. Chem. Phys. 36 (1962) 958.
[6] I.W. Watkins, J. Mol. Spectry. 29 (1969) 402;
E.V. Doktorov, J.A. Malkin and V.I. Manko, J. Mol. Spectry. 56 (1975) 1.
[7] C. Lalo and C. Vermeil, J. Photochem. 3 (1975) 441; 1 (1972/73) 321.
[8] J. Heicklen, N. Kelly and K. Partymiller, Rev. Chem. Intermediates 3 (1980) 315;
E.K.C. Lee and G.L. Loper, in: Radiationless Transitions, ed. S.H. Lin (Academic Press, New York, 1980).
[9] M.W. Wilson, M. Rothschild, D.F. Muller and C.K. Rodes, J. Chem. Phys. 77 (1982) 1837.
[10] C. Fotakis, A. Torre and R.J. Donovan, J. Photochem. 23 (1983) 103.
[11] J. Wildt, E.H. Fink, R. Winter and F. Zabel, Chem. Phys. 80 (1983) 167.
[12] T. Venkitachalam and R. Bersohn, J. Photochem. 26 (1984) 65.
[13] R.K. Sparks, K. Shobatake, L.R. Carlson and Y.T. Lee, J. Chem. Phys. 75 (1981) 3838.
[14] JANAF Thermochemical Tables, J. Phys. Chem. Ref. Data 14 (1985) Suppl. 1.
[15] M. Bielefeld, G. Elfers, E.H. Fink, H. Kruse, J. Wildt, R. Winter and F. Zabel, J. Photochem. 25 (1984) 419.
[16] H. Kanamori, J.E. Butler, K. Kawaguchi, C. Yamada and E. Hirota, J. Mol. Spectry. 113 (1985) 262.
[17] H. Kanamori, E. Tiemann and E. Hirota, J. Chem. Phys. 89 (1988) 621.
[18] J.C. Burkholder, E.R. Lovejoy, P.D. Hammer, C.J. Howard and M. Mizushima, J. Mol. Spectry. 124 (1987) 379.
[19] Y.-P. Lee and G.C. Pimentel, J. Chem. Phys. 69 (1978) 3063.
[20] D.E. Tevault and R.R. Smardzewski, J. Chem. Phys. 69 (1978) 3182.
[21] W.C. Swope, Y.-P. Lee and H.F. Schaefer III, J. Chem. Phys. 71 (1979) 3761.
[22] C.S. Effenhauser, P. Felder and J.R. Huber, J. Phys. Chem. 94 (1990) 296.